Scripta Materialia 254 (2025) 116319

Contents lists available at ScienceDirect

Scripta Materialia

journal homepage: www.journals.elsevier.com/scripta-materialia

Thermal stability of 3D interface Cu/Nb nanolaminates

Justin Y. Cheng [a], Zezhou Li [b], David L. Poerschke [a], J. Kevin Baldwin [c], Brady L. Bresnahan [a], Nathan A. Mara [a,*]

[a] Chemical Engineering and Materials Science, University of Minnesota, MN 55455, United States
[b] Materials Science and Engineering, Beijing Institute of Technology
[c] Center for Integrated Nanotechnologies, Los Alamos National Laboratory, NM 87545, United States

ARTICLE INFO

Keywords:
3D interfaces
Nanocrystalline alloys
Thermal stability
TEM
Nanomechanics

ABSTRACT

Nanocrystalline alloys are promising structural materials yet lack thermal stability in many cases. Recent work shows that interface structure has an outsize effect on the thermal behavior of nanostructured alloys. This work focuses on the role of controlled heterophase interface structure in the thermal evolution of model Cu/Nb nanolaminates. We introduce 3D interfaces containing nanoscale heterogeneities in all spatial dimensions between Cu and Nb, forming 3D Cu/Nb. TEM, nanoindentation, and DSC are used in tandem to establish thermal stability and to identify shifts in microstructure as a function of static annealing temperature. 3D interfaces are shown to survive annealing to 300 °C for 1 hr., while 3D Cu/Nb microstructure evolves to form low-density and voided regions correlating to the onset of layer pinch-off between 500 and 600 °C annealing temperatures. A diffusivity- and vacancy energetics-based mechanism is developed to explain void formation driven by 3D interface degradation at elevated temperature.

The thermal stability of nanostructured alloys is of great interest due to their potential as high-strength structural materials [1–3]. Often, nanocrystalline alloys have low thermal stability, limiting their application [4–6]. Many strategies can enhance nanocrystalline thermal stability, such as grain boundary segregation [7,8], or the inclusion of second phases [9–11] or large quantities of twin boundaries [12,13]. Each method harnesses interface content and structure to improve thermal stability by controlling transport phenomena. Progress in this field requires further fundamental understanding of interface-dominated high temperature microstructure evolution. The current work elucidates this topic by studying the effect of heterophase interfaces with controlled structure on the thermal stability of a model nanolaminated Cu/Nb composite (henceforth Cu/Nb).

Cu/Nb serves as a model system with controlled grain size, morphology, and orientation in which heterophase interface structure dominates properties [14–19]. Cu/Nb has been made with nanoscale layer thickness as thin films using physical vapor deposition [20] (PVD) and in bulk using accumulative roll-bonding [21] (ARB). PVD Cu/Nb thermal stability studies show that layer thickness h determines Cu/Nb thermal stability [17,18]. ARB Cu/Nb studies demonstrate that interface structure can be tailored by thermomechanical processing [22,23] and show that different interface structures produce different thermal stabilities [19]. This demonstrates that interface structure dominates thermal behavior in Cu/Nb at nanoscale layer thicknesses. These prior works also establish that changes in Cu/Nb nanohardness after annealing correlate well with thermally-induced microstructure evolution [17,18].

The thermal evolution of Cu/Nb is determined by interface energetics, where relative heterophase interface and grain boundary energies determine microstructural stability and evolution [17,18]. Prior studies focused on atomically sharp Cu/Nb heterophase interfaces [24–26], which are called “2D interfaces” due to their limited thickness. This work studies Cu/Nb with few-nm thick “3D interfaces” to form a composite called 3D Cu/Nb. 3D interfaces contain chemical, crystallographic, and structural heterogeneities on the length scale of a few nm [27–29]. While 3D interfaces are evocative of thick grain boundaries used to stabilize nanostructures elsewhere [30–32], these other studies involved homogeneous interfaces in equiaxed, non-model microstructures. 3D Cu/Nb is used here to study 3D interface behavior in a model nanolaminate microstructure. 3D heterophase interfaces enhance mechanical performance in Cu/Nb [27,28,33,34], but their thermal stability has not been explored. Furthermore, since some metallic nanostructures can coarsen even at room temperature [35–37], the thermal stability of 3D interfaces must be established to ensure

* Corresponding author.
E-mail address: mara@umn.edu (N.A. Mara).

https://doi.org/10.1016/j.scriptamat.2024.116319
Received 14 February 2024; Received in revised form 8 August 2024; Accepted 14 August 2024
Available online 26 August 2024

repeatability of microstructural and mechanical characterization. Here, 3D interface thermal stability is quantified after *ex situ* annealing with transmission electron microscopy (TEM), nanoindentation, and differential scanning calorimetry (DSC). Microstructure development is presented as a function of annealing temperature and is explained by comparing self-diffusivity of Cu and Nb to vacancy diffusivity.

PVD-grown 3D Cu/Nb with pure layer thickness of 10 nm and interface thickness of 10 nm (10–10 Cu/Nb) was statically annealed in this work to assess its thermal stability. The synthesis details for this material can be found elsewhere [28]. 3D Cu/Nb thin films supported by single crystal Si substrates with 2 μm thickness were encapsulated under rough vacuum in quartz tubing and then annealed at 300, 400, 500, and 600 °C for 1 hr. at each temperature. A Lindberg/Blue M™ BF51442C box furnace was pre-heated to the desired annealing temperature, then an encapsulated specimen was put in the hot furnace. At the end of annealing, encapsulated specimens were placed on fire brick at ambient temperature to rapidly cool. The thermal stability of 3D interfaces was determined by multiple methods. *Ex situ* microstructural characterization was conducted via cross-sectional TEM in an FEI Tecnai T12 operating at 120 kV and a Thermo Fisher F200X Talos operating at 200 kV in parallel beam mode. Scanning TEM (STEM) was also conducted in the Talos. TEM specimens were produced using a FEI Helios Nanolab G4 FIB/SEM. Nanoindentation in post-annealed samples was conducted using a Hysitron TI 980 triboindenter. Nanohardness was measured using the Oliver-Pharr method with a Berkovich tip whose tip area function was calibrated to fused silica [38]. Ten indents per specimen were conducted in load control using a constant strain rate load function with continuous stiffness measurement enabled. A constant indentation strain rate of 5×10^{-2}/s (using $\frac{1}{2}\frac{\dot{P}}{P}$, where P is indentation load [39,40]) was used from 200 to 12,000 μN, the CSM frequency was 200 Hz, and the displacement amplitude was maintained near 1 nm. Representative hardness values for each indent were calculated by averaging the measured hardness across indentation depths over which hardness data was constant. Lastly, differential scanning calorimetry was performed on free-standing 10 μm 10–10 Cu/Nb films in a Netzch STA 449 calorimeter up to 600 and 950 °C at a heating rate of 10 °C/min under a Ti-gettered argon atmosphere. For the 950 °C specimen, a Zr getter ring was placed close to the sample crucible to further suppress specimen oxidation. TEM was also performed on specimens that underwent DSC measurements.

Conventional TEM (CTEM) reveals the thermal evolution of 3D interfaces in Fig. 1. Fig. 1(a) shows that 3D interfaces in the as-deposited 10–10 Cu/Nb can be distinguished from abutting layers by diffraction contrast. After 300 °C annealing in Fig. 1(b), 3D interfaces are still distinguishable from the abutting material. Fig. 1(c) shows that annealing at 400 °C makes 3D interfaces difficult to distinguish from surrounding material. Finally, at 500 °C (Fig. 1(d)), the 3D interfaces cannot be discerned at conventional magnification. Thermal grooving is observed at triple grain junctions, indicating significant atomic mobility during annealing. Increasing the annealing temperature to 600 °C causes disruption of the lamellar microstructure (Fig. 1(e)), which signals the onset of runaway microstructure coarsening [17,41]. Layer pinch-off is observed in Fig. 1(e) and is representative of a larger area of material as shown in Figure S1(a). CTEM observations thus establish that 3D interfaces begin to degrade at 300–400 °C. By 500–600 °C, the 3D interfaces degrade completely and the lamellar microstructure begins to break down.

High-resolution TEM (HRTEM) found in Fig. 2 (a-d) shows as-deposited and thermally degraded 10–10 Cu/Nb at the nanoscale. Fig. 2(a) depicts the as-deposited 10–10 Cu/Nb, demonstrating significant amorphous content in 3D interfaces. The presence of this amorphous content is corroborated by recent nanobeam diffraction characterization of 3D Cu/Nb [34]. The difference in crystallography between pure layers and the 3D interfaces gives rise to the diffraction

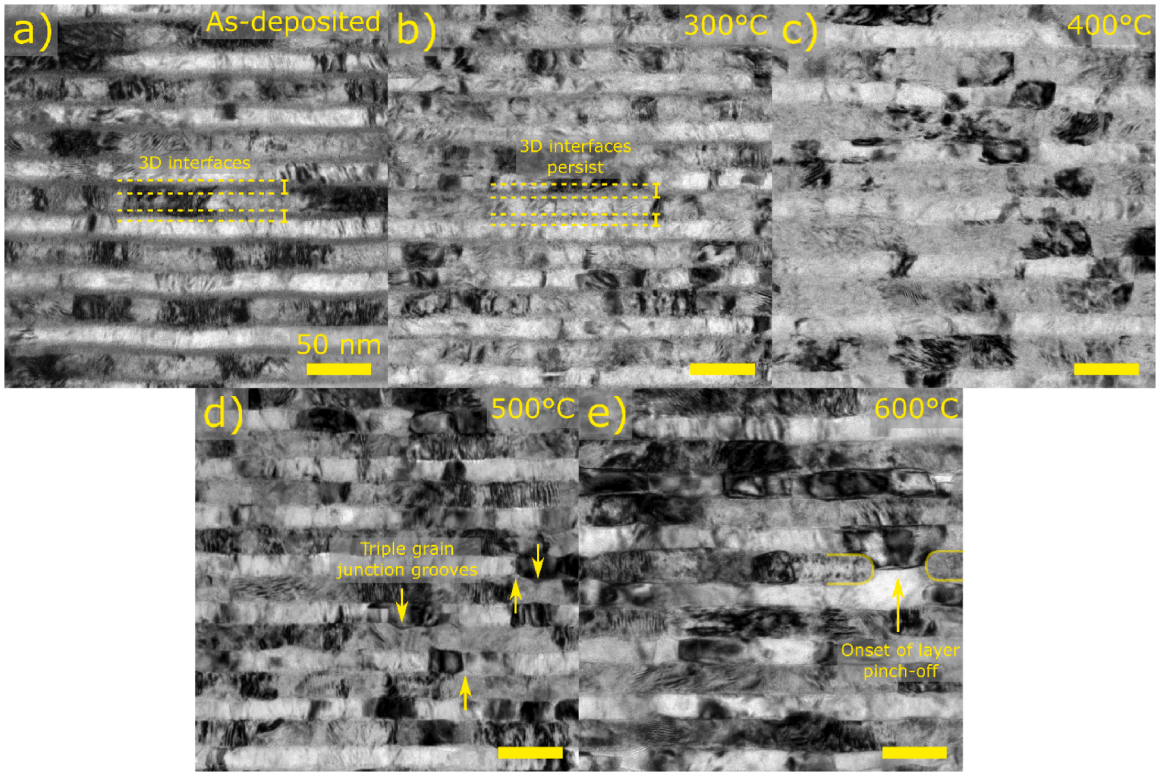

Fig. 1. CTEM micrographs of 10–10 Cu/Nb in the a) as-deposited and (b-e) annealed conditions. Annealing was conducted at b) 300 °C, c) 400 °C, d) 500 °C and e) 600 °C for 1 hour. a) demonstrates the diffraction contrast associated with 3D interfaces found in between pure layers. b) shows that at 300 °C, 3D interfaces persist. c) At 400 °C, 3D interfaces become difficult to distinguish. d) Onset of thermal degradation manifests as triple grain junction grooves after 500 °C annealing. e) Layer pinch-off begins after 600 °C annealing, after which runaway recrystallization should occur [18]. Scale bars are shared between (a-e).

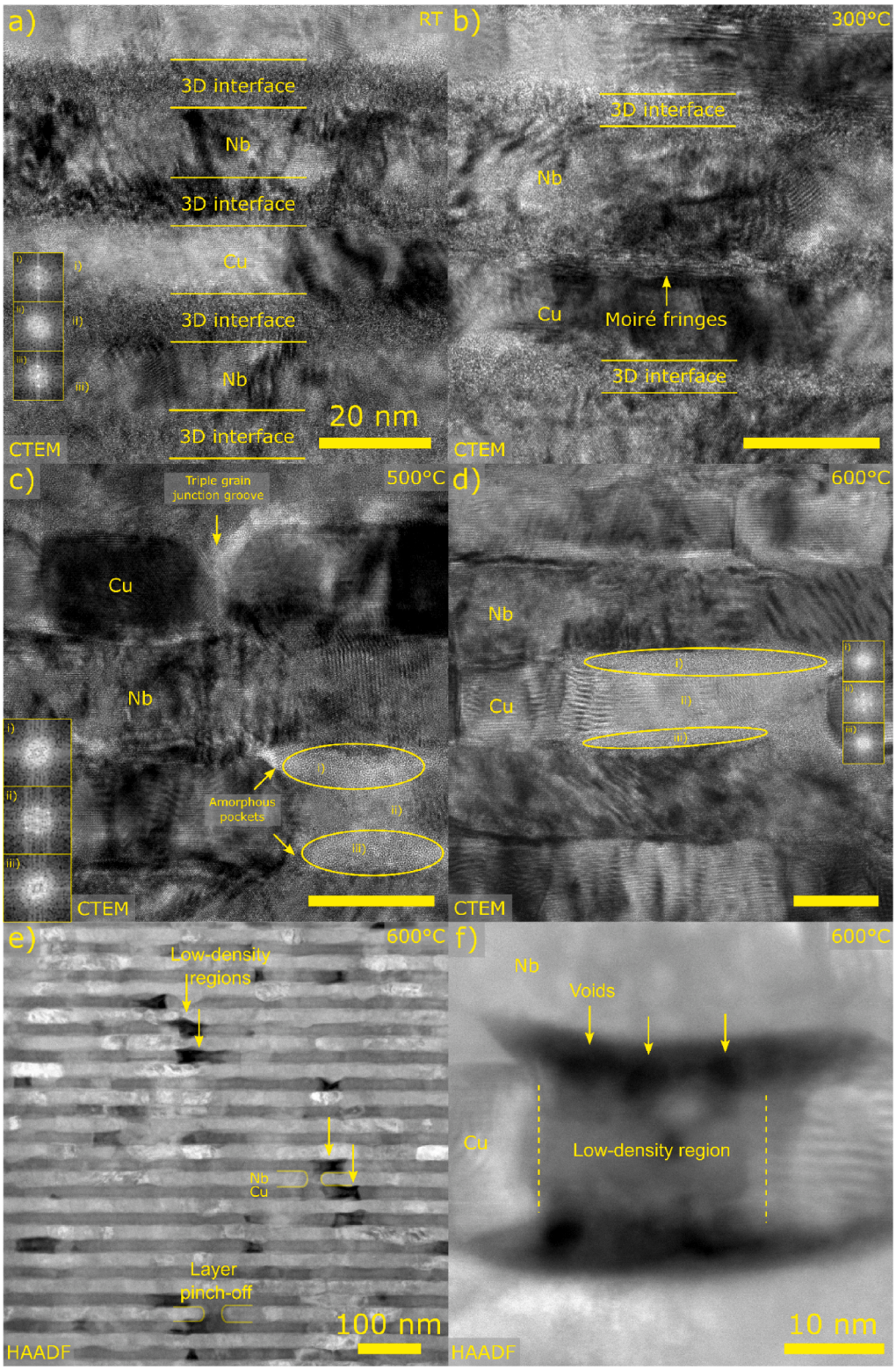

Fig. 2. HRTEM of a) as-deposited 10–10 Cu/Nb and after b) 300 °C, c) 500 °C and d) 600 °C annealing. a) presents the microstructure of the nanolaminate with as-deposited 3D interfaces, which can be distinguished by distinct phase contrast from abutting layers. FFTs taken from regions (i-iii) show that Cu and Nb layers are crystalline, while 3D interfaces contain significant amorphous content. In b), the 3D interface structure is preserved between some layers after 300 °C annealing, while between others Moiré fringes develop. This is due to overlap of pre-existing grains that coarsened at the expense of the 3D interface. c) shows the formation of apparently amorphous pockets abutting a crystal in (i-iii) as a result of 500 °C annealing. d) At 600 °C, regions indicated by (i-iii) consist of amorphous-appearing material abutting crystalline material. e) Z-contrast dominated HAADF STEM micrograph of 600 °C material reveals the presence of low-density regions in the Cu layer where layers appear discontinuous (indicated by arrows). Complete layer pinch-off is found in the Nb layers, which appear brighter than Cu layers in Z-contrast. f) A high-magnification HAADF micrograph of a low-density region corresponding to amorphous-like regions in (c-d). Voids can be discerned in the low-density pockets abutting the low-density grain in the Cu layer. Highlights and shadows were adjusted to improve void contrast in (f). Scale bars are shared between (a-d) and represent 20 nm.

contrast seen in Fig. 1(a). Fig. 2(b) shows detail of 3D interfaces after 300 °C annealing. Some interfaces appear to be mostly unchanged from the as-deposited condition. However, some signatures of thermal degradation are present, such as the Moiré fringes found in between two pure layers. These result from the overlap of pure layer grains grown at the expense of the 3D interface. Fig. 2(c) demonstrates the effect of 500 °C annealing on 10–10 Cu/Nb, which completely degrades the initial 3D interface microstructure. A new microstructural feature formed by annealing is shown in Fig. 2 (c.i-iii), where two apparently amorphous regions sandwich a thin crystalline region. Similar features can be found after annealing at 600 °C in Fig. 2 (d.i-iii). Further examination using high angle annular dark field scanning TEM (HAADF-STEM, 80–200 mrad acceptance angle to emphasize mass-thickness contrast) in Fig. 2 (e-f) reveals the nature of these features. In Fig. 2(e), pinched-off Nb layers correspond with low-density regions indicated by low image intensity. Higher magnification of one of these regions in Fig. 2(f) demonstrates the presence of voids in the low-density regions. Comparison of Fig. 2(d) and Fig. 2(f) shows that the amorphous regions in Fig. 2(d) correspond to the void-heavy regions in Fig. 2(f). These features appear amorphous because their porous structure backfills with redeposited amorphous material during the FIB process. Their formation will be discussed below after a discussion of nanoindentation and DSC.

Nanoindentation results on annealed films corroborate TEM evaluation of 10–10 Cu/Nb thermal stability. Previous work indicates that significant drops in hardness can be correlated with annealing-induced microstructural changes [18,25]. Fig. 3 depicts the hardness of 10–10 Cu/Nb subjected to annealing at different temperatures. Nanohardness is stable up to an annealing temperature of 300 °C. Between 300 and 400 °C, hardness drops by about 0.5 GPa. This corresponds to a ~10 % decrease from as-deposited hardness. This is coincident with the start of 3D interface degradation at 400 °C seen in Fig. 1 (b-c) and Fig. 2(b). The link between 3D interface degradation and softening is supported by previous work demonstrating the strengthening effect of 3D interfaces over 2D interfaces in Cu/Nb [28,42]. As annealing progresses to 500 °C, the hardness is preserved by the continued presence of lamellar grains as seen in Fig. 1(d). Finally, a 1 GPa drop in hardness occurs between 500 and 600 °C corresponding to the onset of pinch-off seen in Fig. 1(e) and

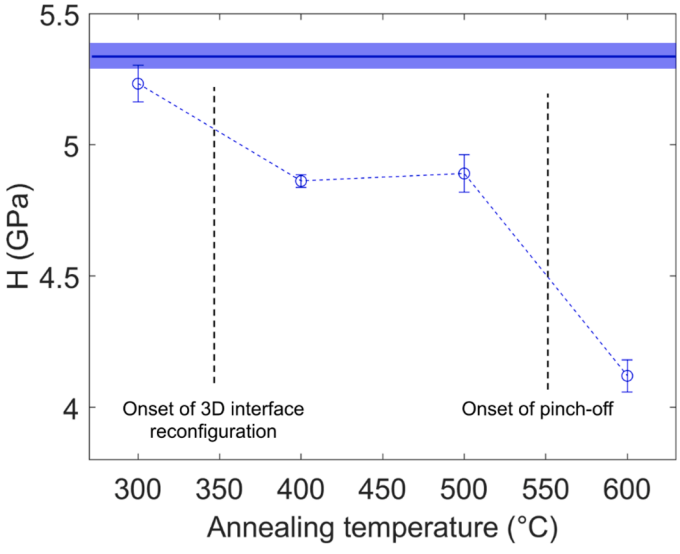

Fig. 3. A plot of nanoindentation hardness as a function of annealing temperature. The as-deposited mean hardness is indicated by a thick blue line, surrounded by blue shading representing one standard deviation to each side. Hardness drops slightly between 300 and 400 °C, suggesting that 3D interface degradation occurs significantly between those temperatures. Hardness drops significantly between 500 and 600 °C, which corresponds to layer pinch-off observed in Fig. 1(e). Error bars represent one standard deviation on each side of mean hardness denoted by open circles.

Fig. 2(e). This is consistent with significant softening correlated with the loss of lamellar microstructure demonstrated in 2D interface Cu/Nb [14].

DSC further quantifies the temperatures corresponding to structural changes in 10–10 Cu/Nb. The DSC trace in Fig. 4 has exothermic features beginning at 500 °C, indicating rapid microstructural rearrangement. The TEM presented in Fig. 1-2 and the nanoindentation in Fig. 3 suggest that the two exothermic peaks from 500 to 900 °C correspond to layer pinch-off at lower temperatures and gross recrystallization or grain growth at higher temperatures. The higher temperature peak is assigned to grain coarsening because large amounts of enthalpy should be released from grain boundaries and heterophase interfaces as the material spheroidizes near melting temperature, which is 1085 °C for Cu [43,44]. The microstructure of the spheroidized material after the higher temperature exothermic peak can be found in Fig. 4(b). It should be noted that oxidation affected the results in Fig. 4 negligibly, as shown by thermogravimetric data in Figure S2.

The data and discussion presented above establishes that 3D interfaces are thermally stable up to 300 °C for 1 hour. This is significant given that 10–10 3D Cu/Nb is nanocrystalline with a very fine effective grain size, the 3D interface structure lacks long range order, and CuNb alloys tend towards dealloying at elevated temperature due to their immiscibility [45]. This stability can be explained by comparison of 3D interfaces to equiatomic CuNb alloys, which tend to be amorphous when cosputtered or quenched [46,47]. 3D interfaces have similar thermal degradation characteristics as amorphous sputtered CuNb alloys, which degrade in the range of 400–500 °C as determined by DSC at 40 °C/min [47].

This work also shows that 2D heterophase interfaces lend greater thermal stability to Cu/Nb than 3D interfaces. PVD Cu/Nb with $h = 75$ nm can survive annealing at 800 °C for 1 h [17], while $h = 15$ nm Cu/Nb completely spheroidizes after 700 °C annealing for 30 min [18]. ARB Cu/Nb also has higher thermal stability than 3D Cu/Nb, surviving 500 °C 1 h annealing at $h = 18$ nm [25]. It should also be noted that static annealing in the current work was conducted on thin films supported by single crystal Si substrates, which give rise to thermal stresses due to thermal expansion mismatch between the film and the substrate. Future work should investigate the role of thermal stresses on thermal stability of 3D interface-containing nanocrystalline alloys.

The thermal evolution of 3D interfaces can be explained by examining mean diffusion lengths of Cu and Nb at elevated temperatures in Table 1. Details of diffusivities and equations used for mean diffusion length calculation can be found in the Supplementary Information [48–50]. These calculations neglect the effect of diffusion along non-lattice pathways such as grain boundaries and 3D interfaces. For example, atomic diffusion is sluggish in CuZr metallic glasses that the amorphous interior of Cu/Nb 3D interfaces resemble [34,51]. Also, fast diffusion through grain boundaries should be considered; Nb undergoes short-circuit diffusion through Cu grain boundaries after annealing at 800 °C for 1 hour [52]. The effect of diffusion along these pathways should be elaborated in future studies.

Table 1 shows that Cu is expected to be solely responsible for atomic migration during annealing of 10–10 Cu/Nb. Nb may be able to migrate through high-diffusivity pathways such as grain boundaries and heterophase interfaces, but should not contribute significant mass transport. The mean diffusion lengths x_{Cu} can be used to understand the behavior of 3D interfaces at different annealing temperatures. Fig. 1-2 show that the 3D interface begins degrading at 300–400 °C. The mechanism of this degradation may stem from growth of Cu and Nb layer grains at the expense of the 3D interface or recrystallization of the 3D interface interior (see Figure S3), but further work must be done to establish this mechanism definitively. x_{Cu} ranges from ~0.5–10 nm between 300 and 400 °C, which is on the order of the 3D interface thickness. This should be sufficient for segregation and recrystallization of Cu from 3D interfaces into abutting Cu grains. At 500–600 °C, x_{Cu} rises beyond 100 nm, meaning that Cu is free to seek thermodynamically favorable sites

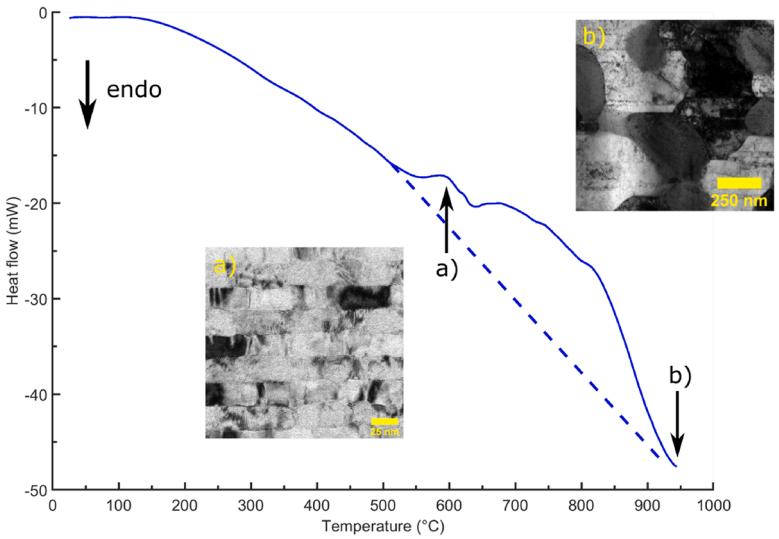

Fig. 4. A DSC heating trace of 10–10 Cu/Nb heated to 950 °C. This curve was created by subtracting heat flow data from a run performed on an empty crucible from the heat flow signal of a run with a crucible containing the Cu/Nb specimen. CTEM micrographs of post-DSC material are included for material heated to a) 600 °C and b) 950 °C. Significant exothermic peaks are found around 600 °C, suggesting that microstructure degradation begins around that temperature. A dashed line is drawn to emphasize the exothermic peaks relative to the baseline trend corresponding to bulk sample heating.

Table 1
Mean diffusion lengths of Cu (x_{Cu}) and Nb (x_{Nb}), and Nb vacancies ($x_{v,Nb}$). The diffusion time is 3600 s, the annealing time used in this study. Arrhenius parameters used for these calculations can be found in Table S1 and the Supplementary Information. x_{Nb} quantities are too small to be physically meaningful, so it can be assumed that bulk self diffusion does not occur appreciably in Nb for the temperatures studied in this work.

Temperature (°C)	x_{Cu} (nm)	x_{Nb} (nm)	$x_{v,Nb}$ (nm)
300	0.487	7.40×10^{-10}	1.23
400	10.5	3.89×10^{-10}	13.0
500	102	4.04×10^{-5}	74.1
600	590	1.45×10^{-3}	284

across multiple layers, leading to the onset of recrystallization and grain coarsening for Cu.

The previous discussion about atom and defect diffusivities reveals a diffusivity mismatch between Cu and Nb at elevated temperatures, suggesting that the Kirkendall effect contributes to the formation of low-density regions and voids at 3D interfaces after 500–600 °C annealing. The diffusivities in Table 1 show that the mismatch of mobilities between Cu and Nb causes volume flux from the Nb-rich side of 3D interfaces as Cu phase segregates, leaving behind Nb vacancies that can migrate far enough to coalesce into voids [53]. This is corroborated by other studies in metallic glasses showing that atomic species diffusivity mismatch causes Kirkendall void formation upon annealing [51,54,55]. In addition, the transformation of any amorphous content in 3D Cu/Nb to crystalline Cu and Nb should inject free volume into the Cu/Nb microstructure in the form of excess atomic free volume. This is because amorphous Cu-Nb alloy has a lower molar volume than the average molar volume of FCC Cu and BCC Nb (as shown by Table S4 [46]). Thus, the voids observed in annealed 3D Cu/Nb have contributions from both the Kirkendall effect and conversion of amorphous material to crystalline.

This work reveals that voids in thermally degraded 3D interfaces do not form uniformly in the interface lateral direction as they do in interdiffusing multilayer systems such as Co/Zr [56]. The voids coalesce preferentially, abutting what appear to be recrystallized grains in Fig. 2 (c-d). Supposing that voids need high energy sites like triple grain junctions or high-energy grain boundaries to nucleate, vacancies must traverse half the in-layer grain size of Cu or Nb grains to coalesce into voids. Other work establishes that the in-layer grain size in 10–10 Cu/Nb is 50–200 nm [33]. At low temperatures, the excess free volume at 3D interfaces is accommodated by vacancies because vacancy diffusivity is low, according to Table 1. Vacancies travel ~1–13 nm at annealing temperatures of 300–400 °C, which is not enough to traverse the Cu/Nb lateral grain size. At higher temperatures vacancy diffusivity is fast enough that excess vacancies can coalesce into voids, lowering the material's free energy [57]. At 500–600 °C, vacancies travel ~75–300 nm, enough to traverse grains laterally and form voids. This means that the voids can only form at 500 °C or above, which matches with TEM observations.

A mechanism explaining the uneven distribution of voids along degraded 3D interfaces in Fig. 5 is presented here. At lower temperatures, Cu in 3D interfaces begins to phase separate into abutting Cu layers, leaving behind Nb- and vacancy-rich interfaces (see Figure S4 for a detailed illustration). At higher temperatures, the 3D interface degrades into a 2D interface and excess vacancies coalesce into void nuclei at energetically favorable sites. As a 2D heterophase interface forms, excess vacancies must migrate from crystalline regions to the heterophase interface since their storage in crystalline Cu and Nb grain interiors would raise the free energy of those phases over equilibrium values. Thus, lateral migration of excess vacancies is constrained to interfaces *en route* to void formation sites. Vacancies are not simply stored at heterophase interfaces because prior elevated temperature irradiation work shows that 2D Cu/Nb heterophase interfaces are poor vacancy sinks compared to other interfaces like in-layer Cu grain boundaries [58]. The high vacancy sink efficiency of high-energy Cu grain boundaries produces local vacancy enrichment, aiding void nucleation at nearby triple-grain junctions [59]. High-energy Cu grain boundaries are not evenly distributed through the material, explaining the non-uniform distribution of thermally-induced voids.

Further thermal evolution gives the microstructures found in Fig. 5 (c-d), which matches Fig. 2 (e-f). Fig. 5 also explains why pinch-off occurs near voided regions as seen in Fig. 2(e). One possible explanation is that Cu and Nb layers constrain each other during thermal degradation, meaning free volume near and in voids can facilitate layer reconfiguration into pinch-off points. Another explanation may be that voids act as vacancy sources that facilitate layer reconfiguration. Excess free volume and vacancies provided by voided regions can aid Nb layer pinch-off (Fig. 1(e) and Fig. 2(e)) despite low bulk diffusivity. Once layer pinch-off happens, runaway grain coarsening can occur [18].

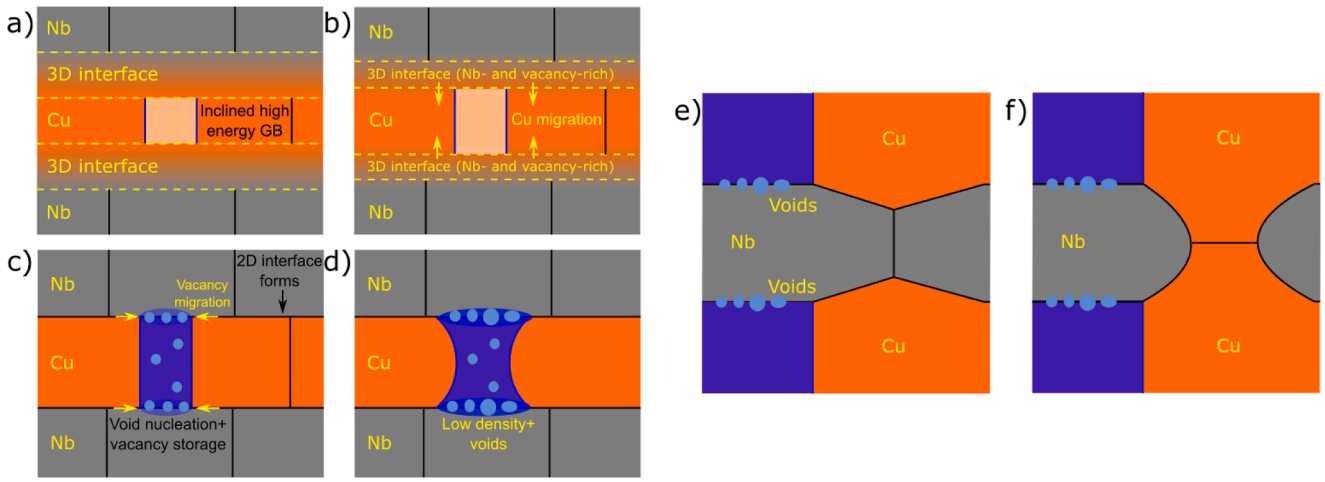

Fig. 5. A schematic diagram of the thermal degradation process in 3D Cu/Nb. (a-d) depict the formation of voids, while (e-f) depict layer pinch-off. a) The as-deposited structure contains 3D interfaces (between yellow dotted lines) and in-plane grain boundaries (black lines). An inclined high energy in-layer Cu grain boundary is indicated by white shading and bounded by dark blue lines. b) At intermediate annealing temperatures (300–400 °C), the 3D interfaces begin to recede and phase separate into abutting pure layers, leaving behind vacancy-rich interfaces. c) Between 400–500 °C, 3D interfaces finish phase separating and vacancy diffusivity is high enough to nucleate voids. Voids, indicated by solid ellipsoids, are driven to high energy sites like triple grain junctions and high energy grain boundaries due to the low vacancy sink efficiency of 2D Cu/Nb interfaces. Regions near voids and at the high-energy Cu grain boundary enrich with vacancies, indicated by blue shading. d) At 500–600 °C, vacancy migration completes, leaving a low-density and voided region. e) Voids near a thermal groove in Nb provide vacancies or free space for Nb layer rearrangement. f) The Nb layer pinches off, allowing contact between two subsequent Cu layers.

In conclusion, this work quantifies the thermal stability of Cu/Nb nanolaminates with 3D interface structure. These composites can survive up to 300–400 °C without loss of lamellar microstructure or significant loss of hardness. This is supported by multiple characterization methods such as static annealing, nanoindentation, and DSC. Further TEM characterization demonstrates the mechanism of thermal degradation in 10–10 Cu/Nb, where voids abut layer pinch-off locations after annealing at 500–600 °C. This behavior was not seen in previous 2D Cu/Nb studies, indicating that 3D interfaces can alter the kinetics of thermal degradation in nanocrystalline alloys dramatically. While 3D interfaces in immiscible systems like Cu-Nb are not expected to be thermally stable, the physics of their thermal degradation elucidated here will shed light on future efforts to understand and pursue high-temperature stability in nanostructured alloys.

CRediT authorship contribution statement

Justin Y. Cheng: Writing – review & editing, Writing – original draft, Visualization, Methodology, Investigation, Formal analysis. **Zezhou Li:** Writing – review & editing, Visualization, Methodology, Investigation. **David L. Poerschke:** Writing – review & editing, Visualization, Supervision, Resources, Methodology, Investigation. **J. Kevin Baldwin:** Writing – review & editing, Investigation. **Brady L. Bresnahan:** Writing – review & editing, Investigation. **Nathan A. Mara:** Writing – review & editing, Supervision, Resources, Project administration, Methodology, Funding acquisition, Conceptualization.

Declaration of competing interest

The authors declare that they have no known competing financial interests or personal relationships that could have appeared to influence the work reported in this paper.

Acknowledgements

This work was supported by DOE BES DE-SC0020133 Office of Science, Basic Energy Sciences. J.Y. Cheng was supported in part by DOE NNSA SSGF under cooperative agreement number DE-NA0003960. Parts of this work were carried out in the Characterization Facility, University of Minnesota, which receives partial support from the NSF through the MRSEC (Award Number DMR-2011401) and the NNCI (Award Number ECCS-2025124) programs. This work was performed, in part, at the Center for Integrated Nanotechnologies, an Office of Science User Facility operated for the U.S. Department of Energy (DOE) Office of Science. Los Alamos National Laboratory, an affirmative action equal opportunity employer, is managed by Triad National Security, LLC for the U.S. Department of Energy's NNSA, under contract 89233218CNA000001. Figures were generated using ImageJ, Inkscape, and the Matlab package export_fig [60].

Supplementary materials

Supplementary material associated with this article can be found, in the online version, at doi:10.1016/j.scriptamat.2024.116319.

References

[1] H. Van Swygenhoven, J.R. Weertman, Deformation in nanocrystalline metals, Mater. Today 9 (2006) 24–31.
[2] C.A. Volkert, E.T. Lilleodden, D. Kramer, J. Weissmüller, Approaching the theoretical strength in nanoporous Au, Appl. Phys. Lett. 89 (2006) 1–4.
[3] Y. Li, D. Raabe, M. Herbig, P.P. Choi, S. Goto, A. Kostka, H. Yarita, C. Borchers, R. Kirchheim, Segregation stabilizes nanocrystalline bulk steel with near theoretical strength, Phys. Rev. Lett. 113 (2014) 106104.
[4] T. Chookajorn, H.A. Murdoch, C.A. Schuh, Design of Stable Nanocrystalline Alloys, Science 337 (2012) 951–954.
[5] J.R. Weertman, Retaining the nano in nanocrystalline alloys, Science 337 (2012) 921–922.
[6] K.D. Ralston, D. Fabijanic, N. Birbilis, Effect of grain size on corrosion of high purity aluminium, Electrochim. Acta 56 (2011) 1729–1736.
[7] P. Lu, F. Abdeljawad, M. Rodriguez, M. Chandross, D.P. Adams, B.L. Boyce, B. G. Clark, N. Argibay, On the thermal stability and grain boundary segregation in nanocrystalline PtAu alloys, Materialia 6 (2019).
[8] J.R. Trelewicz, C.A. Schuh, Grain boundary segregation and thermodynamically stable binary nanocrystalline alloys, Phys. Rev. B - Condens. Matter Mater. Phys. 79 (2009) 1–13.
[9] A. Devaraj, W. Wang, R. Vemuri, L. Kovarik, X. Jiang, M. Bowden, J.R. Trelewicz, S. Mathaudhu, A. Rohatgi, Grain boundary segregation and intermetallic precipitation in coarsening resistant nanocrystalline aluminum alloys, Acta Mater 165 (2019) 698–708.
[10] D.G. Morris, M.A. Morris, Microstructure and strength of nanocrystalline copper alloy prepared by mechanical alloying, Acta Metall. Mater. 39 (1991) 1763–1770.
[11] F. Zhou, J. Lee, E.J. Lavernia, Grain growth kinetics of a mechanically milled nanocrystalline Al, Scr. Mater. 44 (2001) 2013–2017.

[12] O. Anderoglu, A. Misra, H. Wang, X. Zhang, Thermal stability of sputtered Cu films with nanoscale growth twins, J. Appl. Phys. 103 (2008).
[13] S. Zhao, R. Zhang, Q. Yu, J. Ell, R.O. Ritchie, A.M. Minor, Cryoforged nanotwinned titanium with ultrahigh strength and ductility, Science 373 (2021) 1363–1368.
[14] A. Misra, J.P. Hirth, R.G. Hoagland, Length-scale-dependent deformation mechanisms in incoherent metallic multilayered composites, Acta Mater 53 (2005) 4817–4824.
[15] N.A. Mara, D. Bhattacharyya, J.P. Hirth, P. Dickerson, A. Misra, Mechanism for shear banding in nanolayered composites, Appl. Phys. Lett. 97 (2010).
[16] J.S. Carpenter, R.J. McCabe, J.R. Mayeur, N.A. Mara, I.J. Beyerlein, Interface-Driven Plasticity: The Presence of an Interface Affected Zone in Metallic Lamellar Composites, Adv. Eng. Mater. 17 (2015) 109–114.
[17] A. Misra, R.G. Hoagland, H. Kung, Thermal stability of self-supported nanolayered Cu/Nb films, Philos. Mag. 84 (2004) 1021–1028.
[18] A. Misra, R.G. Hoagland, Effects of elevated temperature annealing on the structure and hardness of copper/niobium nanolayered films, J. Mater. Res. 20 (2005) 2046–2054.
[19] S. Zheng, J.S. Carpenter, R.J. McCabe, I.J. Beyerlein, N.A. Mara, Engineering Interface Structures and Thermal Stabilities via SPD Processing in Bulk Nanostructured Metals, Sci. Rep. 4 (2014) 4226.
[20] T.E. Mitchell, Y.C. Lu Jr., A.J. G, M. Nastasi, H Kung, Structure and Mechanical Properties of Copper/Niobium Multilayers, J. Am. Ceram. Soc. 80 (1997) 1673–1676.
[21] J.S. Carpenter, S.C. Vogel, J.E. Ledonne, D.L. Hammon, I.J. Beyerlein, Bulk texture evolution of Cu – Nb nanolamellar composites during accumulative roll bonding, Acta Mater 60 (2012) 1576–1586.
[22] J.S. Carpenter, R.J. McCabe, S.J. Zheng, T.A. Wynn, N.A. Mara, I.J. Beyerlein, Processing Parameter Influence on Texture and Microstructural Evolution in Cu-Nb Multilayer Composites Fabricated via Accumulative Roll Bonding, Metall. Mater. Trans. A 45 (2014) 2192–2208.
[23] J.Y. Cheng, M. Radhakrishnan, C. Miller, R. Mier, S.C. Vogel, D.J. Savage, J. S. Carpenter, O. Anderoglu, N.A. Mara, The Influence of Thermomechanical Treatment Pathways on Texture and Mechanical Properties in ARB Cu/Nb Nanolaminates, Mater. Sci. Eng. A (2023). In press.
[24] K. Yu-Zhang, J.D. Embury, K. Han, A. Misra, Transmission electron microscopy investigation of the atomic structure of interfaces in nanoscale Cu-Nb multilayers, Philos. Mag. 88 (2008) 2559–2567.
[25] J.S. Carpenter, S.J. Zheng, R.F. Zhang, S.C. Vogel, I.J. Beyerlein, N.A. Mara, Thermal stability of Cu-Nb nanolamellar composites fabricated via accumulative roll bonding, Philos. Mag. 93 (2013) 718–735.
[26] I.J. Beyerlein, N.A. Mara, J. Wang, J.S. Carpenter, S.J. Zheng, W.Z. Han, R. F. Zhang, K. Kang, T. Nizolek, T.M. Pollock, Structure–Property–Functionality of Bimetal Interfaces, JOM 64 (2012) 1192–1207.
[27] Y. Chen, N. Li, R.G. Hoagland, X.Y. Liu, J.K. Baldwin, I.J. Beyerlein, J.Y. Cheng, N. A. Mara, Effects of three-dimensional Cu/Nb interfaces on strengthening and shear banding in nanoscale metallic multilayers, Acta Mater 199 (2020) 593–601.
[28] J.Y. Cheng, S. Xu, Y. Chen, Z. Li, J.K. Baldwin, I.J. Beyerlein, N.A. Mara, Simultaneous High-Strength and Deformable Nanolaminates With Thick Biphase Interfaces, Nano Lett 22 (2022) 1897–1904.
[29] Z. Li, J.Y. Cheng, J.D. Poplawsky, S. Xu, J.K. Baldwin, I.J. Beyerlein, N.A. Mara, Critical length scales for chemical heterogeneity at Cu/Nb 3D interfaces by atom probe tomography, Scr. Mater. 223 (2023) 115078.
[30] J. Ding, Z. Shang, Y.F. Zhang, R. Su, J. Li, H. Wang, X. Zhang, Tailoring the thermal stability of nanocrystalline Ni alloy by thick grain boundaries, Scr. Mater. 182 (2020) 21–26.
[31] A. Khalajhedayati, T.J. Rupert, High-Temperature Stability and Grain Boundary Complexion Formation in a Nanocrystalline Cu-Zr Alloy, Jom 67 (2015) 2788–2801.
[32] S.J. Dillon, M. Tang, W.C. Carter, M.P. Harmer, Complexion: A new concept for kinetic engineering in materials science, Acta Mater 55 (2007) 6208–6218.
[33] J.Y. Cheng, J. Wang, Y. Chen, S. Xu, J.G. Barriocanal, J.K. Baldwin, I.J. Beyerlein, N.A. Mara, 3D interfaces enhance nanolaminate strength and deformability in multiple loading orientations, Acta Mater 267 (2024) 119697.
[34] J.Y. Cheng, The Influence of 3D Interfaces on Mechanical Behavior of Nanolaminated Bimetallic Composites, University of Minnesota, 2024.
[35] B. Günther, A. Kumpmann, H.D. Kunze, Secondary recrystallization effects in nanostructured elemental metals, Scr. Metall. Mater. 27 (1992) 833–838.
[36] K. Pantleon, M.A.J. Somers, In situ investigation of the microstructure evolution in nanocrystalline copper electrodeposits at room temperature, J. Appl. Phys. 100 (2006).
[37] M. Ames, J. Markmann, R. Karos, A. Michels, A. Tschöpe, R. Birringer, Unraveling the nature of room temperature grain growth in nanocrystalline materials, Acta Mater 56 (2008) 4255–4266.
[38] W.C. Oliver, G.M. Pharr, Measurement of hardness and elastic modulus by instrumented indentation: Advances in understanding and refinements to methodology, J. Mater. Res. 19 (2004) 3–20.
[39] B.N. Lucas, W.C. Oliver, Indentation power-law creep of high-purity indium, Metall. Mater. Trans. A 30 (1999) 601–610.
[40] K.M. Schmalbach, N.A. Mara, Algorithms for Nanoindentation Strain Rate Jump Testing and Analysis, Exp. Mech. 62 (2022) 885–888.
[41] A.C. Lewis, D. Josell, T.P. Weihs, Stability in thin film multilayers and microlaminates: The role of free energy, structure, and orientation at interfaces and grain boundaries, Scr. Mater. 48 (2003) 1079–1085.
[42] Y. Chen, N. Li, R.G. Hoagland, X.Y. Liu, J.K. Baldwin, I.J. Beyerlein, J.Y. Cheng, N. Mara, Effects of three-dimensional Cu/Nb interfaces on strengthening and shear banding in nanoscale metallic multilayers, Acta Mater 199 (2020) 593–601.
[43] C. Michaelsen, K. Barmak, T.P. Weihs, Investigating the thermodynamics and kinetics of thin film reactions by differential scanning calorimetry, J. Phys. D. Appl. Phys. 30 (1997) 3167–3186.
[44] W.M. Haynes, CRC Handbook of Chemistry and Physics, CRC press, 2016.
[45] C. Michaelsen, C. Gente, R. Bormann, The thermodynamics of amorphous phases in immiscible systems: The example of sputter-deposited Nb–Cu alloys, J. Appl. Phys. 81 (1997) 6024–6030.
[46] S. Xu, J.Y. Cheng, Z. Li, N.A. Mara, I.J. Beyerlein, Phase-field modeling of the interactions between an edge dislocation and an array of obstacles, Comput. Methods Appl. Mech. Eng. 389 (2022) 114426.
[47] C. Michaelsen, C. Gente, R. Bormann, The thermodynamics of amorphous phases in immiscible systems: The example of sputter-deposited Nb-Cu alloys, J. Appl. Phys. 81 (1997) 6024–6030.
[48] K. Maier, Self-diffusion in copper at “low” temperatures, Phys. Status Solidi 44 (1977) 567–576.
[49] T.S. Lundy, F.R. Winslow, R.E. Pawel, C.J. Mchargue, Diffusion of Nb-95 and Ta-182 in Niobium (Columbium), Trans. Metall. Soc. AIME 233 (1965) 1533–1538.
[50] K. Maier, M. Peo, B. Saile, H.E. Schaefer, A. Seeger, High–temperature positron annihilation and vacancy formation in refractory metals, Philos. Mag. A Phys. Condens. Matter, Struct. Defects Mech. Prop. 40 (1979) 701–728.
[51] S.V. Ketov, Y.P. Ivanov, B. Putz, Z. Zhang, J. Eckert, A.L. Greer, Atomic diffusivities in amorphous and liquid Cu-Zr: Kirkendall effects and dependence on packing density, Acta Mater 214 (2021) 116993.
[52] E. Sheu, T.Y. Liu, D.J. Williams, J.K. Baldwin, M.J. Demkowicz, Permeation of niobium through grain boundaries in copper, Acta Mater 274 (2024) 120002.
[53] A.D. Smigelskas, E.O. Kirkendall, Zinc diffusion in alpha brass, Trans. AIME 171 (1947) 130–142.
[54] K.N. Tu, T.C. Chou, Submicron void formation in amorphous NiZr alloys, Phys. Rev. Lett. 61 (1988) 1863–1866.
[55] P. Klugkist, K. Rätzke, F. Faupel, Evidence of Defect-Mediated Zirconium Self-Diffusion in Amorphous Co92Zr8, Phys. Rev. Lett. 81 (1998) 614–617.
[56] H. Schröder, K. Samwer, U. Köster, Micromechanism for metallic-glass formation by solid-state reactions, Phys. Rev. Lett. 54 (1985) 197–200.
[57] D.A. Porter, K.E. Easterling, M.Y. Sherif, Phase Transformations in Metals and Alloys, CRC Press, 2009.
[58] W. Han, M.J. Demkowicz, N.A. Mara, E. Fu, S. Sinha, A.D. Rollett, Y. Wang, J. S. Carpenter, I.J. Beyerlein, A. Misra, Design of radiation tolerant materials via interface engineering, Adv. Mater. 25 (2013) 6975–6979.
[59] W.Z. Han, M.J. Demkowicz, E.G. Fu, Y.Q. Wang, A. Misra, Effect of grain boundary character on sink efficiency, Acta Mater 60 (2012) 6341–6351.
[60] Altman, Y. export_fig (https://github.com/altmany/export_fig/releases/tag/v3.42). GitHub (2023). Available at: https://github.com/altmany/export_fig/releases/tag/v3.42.